Heteroatom Chemistry
Volume 2, Number 3, 1991

# The Syntheses and Structures of Iron Carbonyl Adducts of Tricoordinated Hypervalent Phosphorus Compounds

Anthony J. Arduengo, III,* Michael Lattman,*† David A. Dixon,* and Joseph C. Calabrese

*Contribution No. 5739 from Du Pont Central Research and Development, Experimental Station, Wilmington, Delaware 19880-0328, U.S.A.*

*Received 13 March 1991.*

## ABSTRACT

*The hypervalent phosphorus compound 3,7-di-t-butyl-5-aza-2,8-dioxa-1-phosphabicyclo[3.3.0]octa-2,4,6-triene (ADPO), forms a monosubstituted adduct, ADPO·Fe(CO)$_4$, by direct reaction of 10-P-3 ADPO with Fe$_2$(CO)$_9$ or Fe(CO)$_5$, as well as by reaction of 1,1-dichloro-3,7-di-t-butyl-5-aza-2,8-dioxa-1-phosphabicyclo[3.3.0]octa-3, 6-diene(ADPO·Cl$_2$) with Na$_2$[Fe(CO)$_4$]. The X-ray crystal structure of ADPO·Fe(CO)$_4$ shows that ADPO is coordinated to the iron through the phosphorus. The phosphorus of the adduct has a tetrahedral 8-P-4 geometry in contrast to the planar T-shaped geometry of uncomplexed 10-P-3 ADPO. Ultraviolet photolysis of ADPO·Fe(CO)$_4$ yields the disubstituted species (ADPO)$_2$·Fe(CO)$_3$ wherein ADPO has dimerized via P–O bond cleavage to form a bidentate (ADPO)$_2$ ligand containing a 10-membered ring that bridges axial and equatorial positions at the trigonal bipyramidal iron center.*

## *INTRODUCTION*

We have reported the synthesis [1–5], structure [1–4], chemistry [1–4, 6–11] and electronic structure [4, 12, 13] of unusual ring systems that contain 3-coordinate 10-electron pnictogen centers. For a 10-Pn-3 [14] arrangement, two lone pairs of electrons in equatorial positions are expected at the pnictogen center. Numerous metal complexes of these 5-aza-2,8-dioxa-1-pnictabicyclo[3.3.0]octa-2,4,6-triene (ADPnO) [15] ring systems have been prepared and structurally characterized. [4, 8–11] These metal complexes have allowed the demonstration of chemical [4, 8–10] or stereochemical [4, 8–10] activity of equatorial lone pairs at antimony and arsenic centers. The phosphorus-derived ADPO ring system has been somewhat of an enigma in that the metal chemistry has afforded structures that appear to be derived from the 8-P-3 ADPO rather than 10-P-3 ADPO. Theoretical studies [4, 12] on these ADPnO molecules suggest that the arsenic and antimony compounds can be described by a simple valence bond model for the 10-Pn-3 structures such as that depicted for ADPO in Equation 1. The theoretical models of the phosphorus-derived ADPO system indicate an electronic arrangement similar to the heavier arsenic and antimony analogs. [4, 12] Unlike the heavier analogs there is sufficient overlap between the phosphorus and its adjacent nitrogen and oxygen centers to allow delocalization of a phosphorus lone pair into the ligand $\pi$-system. This delocalization of the phosphorus p-lone pair in 10-P-3 ADPO causes the 8-P-3 and 10-P-3 arrangements to be close in energy: The coordination chemistry of ADPO with transition metal centers has given complexes in which the phosphorus center is found in a tetrahedral 8-P-4 environment as if the complex had been derived from 8-P-3 ADPO. When ADPO is released from these metal complexes

Dedicated to Professor Dr. Marianne Baudler on the occasion of her seventieth birthday.

*To whom correspondence should be addressed.

†Visiting Research Scientist on leave from the Department of Chemistry, Southern Methodist University, Dallas, Texas 75275, U.S.A.



1042-7163/91/$3.50 + .25

by displacement with another ligand the ADPO assumes the 10-P-3 arrangement. We now report adducts of ADPO derived from iron carbonyl in which unique chemistry can be observed for the ADPO ring system.

## *RESULTS*

When a mixture of ADPO and $Fe_2(CO)_9$ in pentane was stirred at ambient temperatures for several hours, the $Fe_2(CO)_9$ slowly dissolved to give the monosubstituted complex ADPO·$Fe(CO)_4$ in virtually quantitative yield (Equation 1).

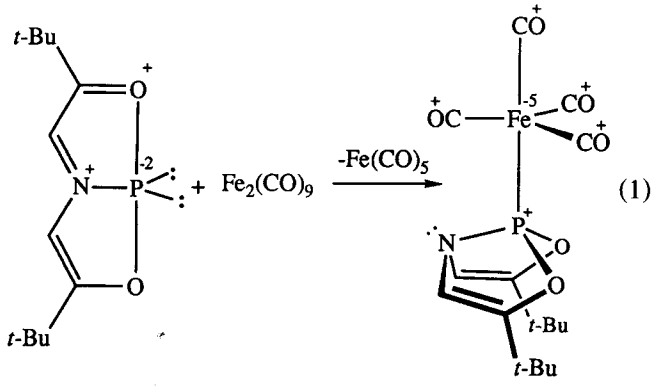


(1)

The $\nu_{CO}$ region in the IR spectrum is typical for an $LFe(CO)_4$ species substituted in the axial position of the iron [16]; however, the bands are at significantly higher frequency compared to other $R_3PFe(CO)_4$ (R = alkyl [17], phenyl [17], $Me_2N$ [18]) species, and even slightly higher than for $(MeO)_3PFe(CO)_4$ [17], suggesting that ADPO is a good $\pi$-acceptor. Coordination of the phosphorus is indicated by the $^{31}P$ NMR ($C_6D_{12}$) chemical shift of $\delta$ 235 and large phosphorus coupling (22.6 Hz) to the carbonyl carbons attached to the iron (these carbons are equivalent on the NMR time scale) [19, 20]. The $^1H$ NMR spectrum shows an upfield shift ($\delta$ 7.50 → 5.89) and increase in $^3J_{PH}$ (9.6 Hz → 26.4) for the ADPO ring protons, compared to uncomplexed 10-P-3 ADPO. An upfield shift ($\delta$ 169.9 → 156.4) for the carbon attached to oxygen in the tridentate ligand of ADPO is revealed in the $^{13}C$ NMR spectrum of ADPO·$Fe(CO)_4$. These data are consistent with a folded 8-electron environment at phosphorus as previously observed for other metal ADPO adducts [11, 4, 8, 9]. A single crystal X-ray analysis confirms the structure of ADPO·$Fe(CO)_4$.

The ADPO ligand in ADPO·$Fe(CO)_4$ is approximately tetrahedral about phosphorus. Coordination to the iron is through the phosphorus. The iron is approximately trigonal bipyramidal (TBP) with ADPO at one of the axial sites (Figure 1). The Fe–P distance (Table 1) is about 8 pm shorter than the corresponding distances in L·$Fe(CO)_4$ (L = $(Me_2N)_3P$ [22], $Ph_3P$ [23], $Ph_2HP$ [24]), and about the same

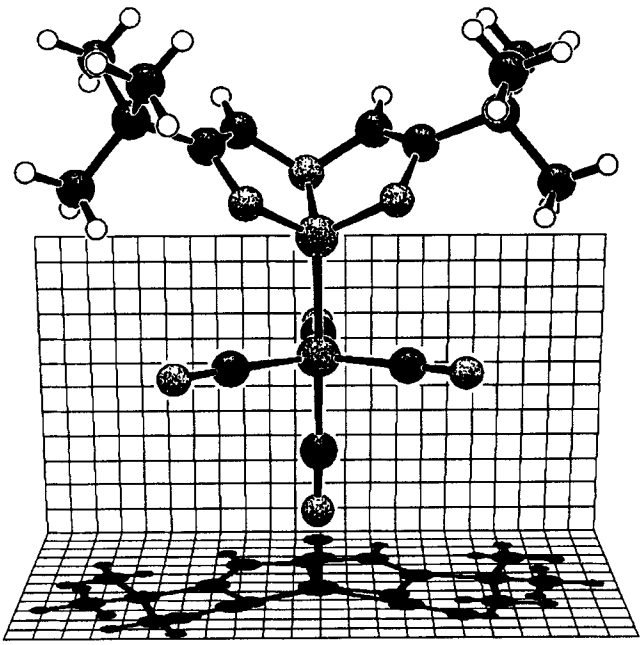

**FIGURE 1** KANVAS [21] drawing of the X-ray structure of ADPO·$Fe(CO)_4$.

as $[(MeNCH_2CH_2NMe)PF]Fe(CO)_4$ [25]. A $Cp(C_6H_5)(CO)Fe$ adduct of a saturated analog of ADPO gives an Fe–P distance of 210.5(2) pm [26]. This Fe–P bond distance in ADPO·$Fe(CO)_4$ may reflect $\pi$-acceptor properties of coordinated ADPO. The Fe–C and C–O bond lengths are typical for these types of complexes [22–25, 27]. The overall ADPO geometry in the complex is very similar to the ADPO ligands in *cis*-$(ADPO)_2PtI_2$ [11]. As expected, the distortion from a planar geometry in free ADPO to a tetrahedral geometry in the complex is accompanied by significant changes in most of the ligand bond lengths. In the complex, the C–O and C–N bonds are longer while the $C–C_{ring}$ bonds are shorter, reflecting the localization of the C=C double bond in the folded structure. The P–O bond lengths have decreased by the greatest amount as a result of the formation of 2-center 2-electron bonds from the hypervalent bond. The P–N bond length remains unaltered.

One remarkable feature of the structure of ADPO·$Fe(CO)_4$ is the conformation of ADPO with respect to the $Fe(CO)_4$ unit; the two P–O and one P–N bonds are virtually eclipsed with the three carbonyls in the equatorial plane of the iron. To our knowledge, all other $R_3PFe(CO)_4$ complexes that have been structurally characterized [22–25, 27] have staggered conformations, presumably to minimize steric interactions. It is tempting to suggest an interaction between the nitrogen and/or oxygen atoms on ADPO with the iron carbonyl fragment, but the absence of significant Fe–C–O bond differences with other complexes argues against this [22–25, 27].

The same ADPO·$Fe(CO)_4$ adduct was obtained

**TABLE 1** Selected Bond Lengths and Angles in ADPO·Fe(CO)$_4$

| *Bond Length (pm)* | | *Bond Angle (deg.)* | |
|---|---|---|---|
| Fe–P | 215.8(3) | C–Fe–P | 175.0(4), 91.1(3), 91.5(3), 86.7(3) |
| Fe–C | 179.7(9), 178.9(10), 179.2(10), 180.0(12) | Fe–P–N | 124.6(3) |
| P–O | 162.3(6), 164.7(6) | Fe–P–O | 114.7(2), 114.6(2) |
| P–N | 170.4(9) | N–P(fold) | 116.5 |
| C–$O_{ADPO}$ | 141.4(11), 144.4(11) | C–C–O | 114.7(8), 115.4(8) |
| C≡O | 114.0(10), 114.6(10) 122.5(11), 114.2(13) | C–C–N | 113.0(10), 114.0(10) |
| | | O–P–O | 108.3(3) |
| | | O–P–N | 95.4(4), 96.3(4) |
| C–N | 145.7(10), 145.7(10) | C–N–C | 115.8(6) |
| C–$C_{ring}$ | 130.1(14), 128.9(14) | C–Fe–P–N | 7.7, 126.2, −113.6 |

when the ADPO fragment originated from a material in which the ADPO backbone is reduced (such as ADPO·$Cl_2$) rather than oxidized as it is in uncomplexed 10-P-3 ADPO. The reaction of ADPO·$Cl_2$ with $Na_2[Fe(CO)_4]$ (Equation 2) produced ADPO·Fe(CO)$_4$, though spectral properties show this reaction not to be as clean (see Experimental section).

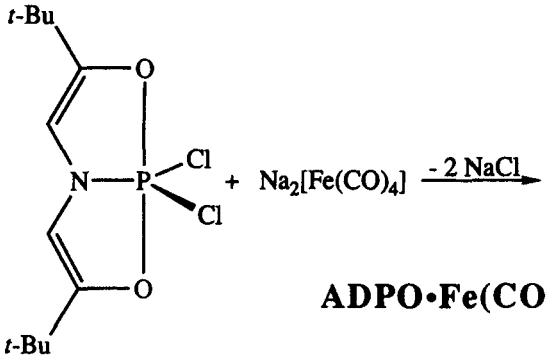


**ADPO·$Cl_2$** **ADPO·Fe(CO)$_4$** (2)

Reaction of ADPO·Fe(CO)$_4$ and ADPO in cyclohexane, under UV irradiation, led to the formation of the disubstituted product (ADPO)$_2$Fe(CO)$_3$ (Equation 3). UV irradiation of (or, alternatively, boiling) a solution containing only (ADPO)Fe(CO)$_4$ yields the identical product. The usual geometry for unconstrained *bis*(phosphorus) iron tricarbonyl complexes is TBP with phosphorus ligands in the axial positions [16, 17, 22, 27]. However, the IR spectrum of (ADPO)$_2$Fe(CO)$_3$ does not show the single major band in the $\nu_{CO}$ region that would be expected for *trans*-$L_2$Fe(CO)$_3$. Rather, three major bands are observed, indicative of a *cis* geometry. (One resonance is observed for the iron carbonyl carbon atoms in the $^{13}$C NMR spectrum, which is split into an apparent triplet by coupling to the phosphorus atoms, suggesting equivalence of the phosphorus atoms and carbonyls on the NMR time scale [19, 20]. The $^{31}$P NMR {$^1$H} ($C_6D_{12}$) spectrum exhibits a single phosphorus resonance at $\delta$ 172. Two resonances are observed in each of the methyl and ethylenic regions of the $^1$H NMR spectrum [28]. The ethylenic protons show an upfield shift from uncomplexed ADPO ($\delta$ 7.50 → 5.58 and 5.94) but the phosphorus couplings remain small (7.4 and 7.0 Hz). These P–H couplings are uncharacteristically small for typical folded ADPO–metal complexes. These NMR and IR observations indicate that the two rings of each ADPO fragment remain inequivalent even though the phosphorus atoms interconvert. The coupling patterns further suggest that the ring structures are different from the previously studied folded ADPO–metal complexes.

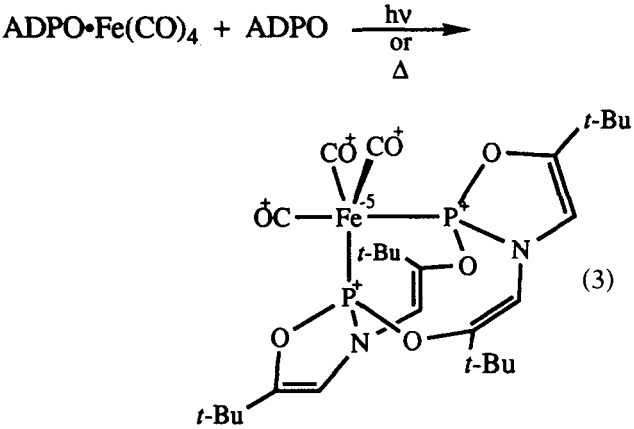


(3)

**(ADPO)$_2$Fe(CO)$_3$**

An X-ray structural characterization of (ADPO)$_2$Fe(CO)$_3$ confirms the axial/equatorial arrangement of the two phosphorus centers (Figure 2). The solid state structure of (ADPO)$_2$Fe(CO)$_3$ reveals that the two ADPO subunits have dimerized via P–O bond cleavage to transform two 5-membered rings into a 10-membered ring. This dimerization is unprecedented in ADPnO chemistry [4, 6, 7]. However, Houalla has reported such dimerizations in completely saturated analogs of the ADPO ring system [29, 30].

The 10-membered ring in (ADPO)$_2$Fe(CO)$_3$ contains two approximately co-planar vinyl-ether/enamine (N–C=C–O) fragments. The great-

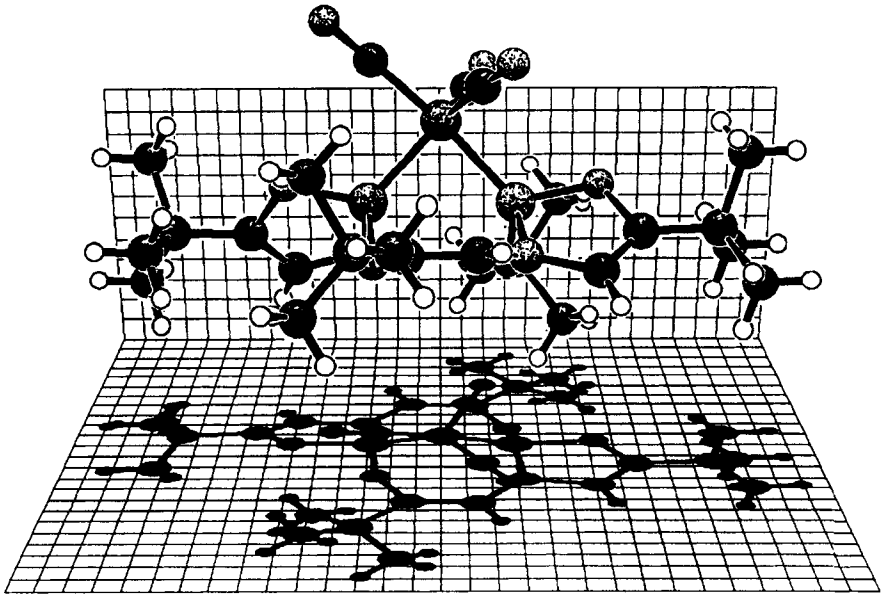

**FIGURE 2** KANVAS [21] drawing of the X-ray structure of $(ADPO)_2Fe(CO)_3$.

est deviation from the mean plane for these eight atoms is 0.12 Å for one of the oxygens. The last two members of the 10-membered ring, the phosphorus atoms, are both 1.04 Å out of the mean plane for the other eight atoms. The direct view in Figure 2 is into the plane of the 10-membered ring, bisecting the C–C double bonds. The outline of the 10-membered ring with the two fused 5-membered rings is visible on the shadowed plane below the structure. The 5-membered rings also contain vinylether/enamine (N–C=C–O) fragments so that each of them is likewise fairly planar. The largest deviation from planarity in the 5-membered rings is ~0.09 Å at the oxygens. The two 5-membered rings are each twisted approximately 40° with respect to the central ring. These features create an approximate $C_2$ symmetry in the ADPO dimer. To accommodate this propeller arrangement each of the nitrogens has pyramidalized slightly (sum of the valence angles is ~353°). The iron tricarbonyl fragment rests over the center of the ring system, along the approximate 2-fold axis, with one phosphorus occupying an axial position and the other occupying an equatorial position.

The bond lengths and angles in $(ADPO)_2Fe(CO)_3$ (Table 2) support the localization of $\pi$-bonding in the ADPO dimer. The bond lengths and angles in the two 5-membered rings follow the trends observed in the previous complexes with folded ADPO [9, 11]. As expected, the bond angles in the 10-membered ring are somewhat larger than their counterparts in the 5-membered rings.

**TABLE 2** Selected Bond Lengths and Angles in $(ADPO)_2Fe(CO)_3$

| *Bond Length (pm)* | | *Bond Angle (deg.)* | |
|---|---|---|---|
| $Fe-P_{ax}$ | 213.32(8) | $C-Fe-P_{ax}$ | 170.9(1), 94.39(9), 86.9(1) |
| $Fe-P_{eq}$ | 212.01(9) | $C-Fe-P_{eq}$ | 88.9(1), 118.8(1), 122.9(1) |
| | | P–Fe–P | 83.93(3) |
| Fe–C | 178.3(3), 178.6(3), 178.2(3) | C–Fe–C | 118.1(1), 94.0(1), 92.3(1) |
| $P-O_{10}$[a] | 163.0(2), 161.1(2) | O–P–O | 101.3(1), 100.5(1) |
| $P-O_5$[a] | 162.5(2), 163.1(2) | $N-P-O_{10}$[a] | 99.8(1), 99.9(1) |
| P–N | 168.0(2), 169.1(2) | $N-P-O_5$[a] | 93.7(1), 92.3(1) |
| $C-O_{10}$[a] | 140.4(3), 139.9(3) | $C-C-O_{10}$[a] | 120.6(2), 120.8(2) |
| $C-O_5$[a] | 140.9(3), 140.7(3) | $C-C-O_5$[a] | 112.2(2), 111.9(2) |
| C≡O | 114.8(4), 114.0(4), 114.7(4) | C–N–C | 120.1(2), 120.3(2) |
| $C-N_{10}$[a] | 142.2(3), 141.4(4) | $C-C-N_{10}$[a] | 126.3(2), 127.2(2) |
| $C-N_5$[a] | 141.9(4), 140.8(4) | $C-C-N_5$[a] | 112.7(2), 112.8(2) |
| $C-C_{10}$[a] | 131.9(4), 132.7(4) | $Pl_5-Pl_{10}$[b] | 40.5, 42.4 |
| $C-C_5$[a] | 133.1(4), 132.7(4) | $Pl_5-Pl_{5'}$[b] | 82.9 |

[a] The subscript 5 or 10 denotes whether the value is from a 5- or 10-membered ring.
[b] The angle between designated mean planes.

$$(ADPO)_2Fe(CO)_3 + ADPO \xrightarrow{h\nu}$$

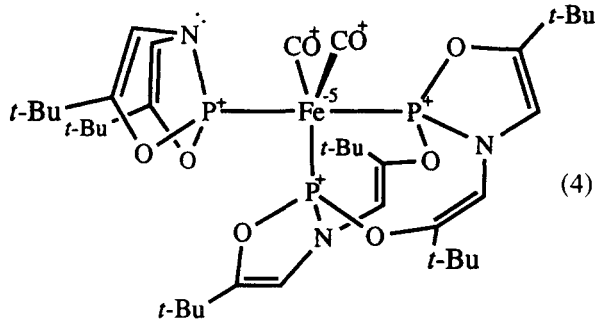

(4)

## $(ADPO)_2Fe(ADPO)(CO)_2$

Further reaction of $(ADPO)_2Fe(CO)_3$ with excess ADPO was attempted. Under UV irradiation a product is formed with two $^{31}P$ resonances, coupled to one another. One resonance appears as a doublet at $\delta$ 174, while the other is a triplet at $\delta$ 240 ($J_{PP}$ = 21.7 Hz). The fact that these resonances are very similar to those of $(ADPO)_2Fe(CO)_3$ and $ADPO{\cdot}Fe(CO)_4$, respectively, suggest that simple coordination of a bent molecule of ADPO has occurred, yielding $(ADPO)_2Fe(ADPO)(CO)_2$ (Equation 4). There seems to be no tendency to form any type of ADPO trimer. Although $(ADPO)_2Fe(ADPO)(CO)_2$ was not isolated, it is easily characterized by its solution NMR spectra. Since the dimeric ADPO unit is chiral with a $C_2$ axis, the third isolated ADPO unit contains diastereotopic *t*-butyls and ethylenic protons. This feature is nicely evident in the $^1H$ NMR spectrum, which exhibits resonances at $\delta$ 1.04 and 1.12 for the *t*-butyls. The new ethylenic protons appear as a set of doublets at $\delta$ 5.55 and 5.62. The magnitude of the phosphorus couplings to the various ethylenic protons (6.9 vs ~25 Hz) supports the isolated nature of the third ADPO unit. Further CO substitution beyond the dicarbonyl was not observed.

When heated under pressure with carbon monoxide, $ADPO{\cdot}Fe(CO)_4$ will release ADPO. As we had previously observed with platinum complexes [11], the liberated ADPO assumes the planar 10-P-3 arrangement with no evidence of folded 8-P-3 ADPO. Attempts to dislodge ADPO or ADPO dimer from $(ADPO)_2Fe(CO)_3$ have been unsuccessful even under 925 atms of carbon monoxide.

## *DISCUSSION*

The formation of a 1:1 adduct between iron carbonyls and ADPO is consistent with theoretical studies of the ADPO system [4, 12] and in accord with previous experimental findings for other transition metal electrophiles [8, 9, 11]. We have recently reported metal adducts of tricoordinate hypervalent pnictogen compounds in which the pnictogen center is coordinated to two metals (**1**) [9]. Structures of the type **1** were observed for arsenic and antimony centers but not phosphorus.

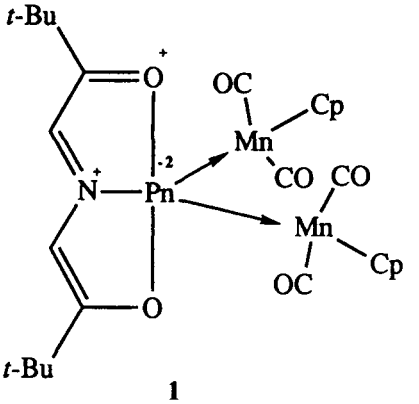

**1**

Although an iron carbonyl precursor can be chosen that contains two iron centers (e.g. $Fe_2(CO)_9$) it was not possible to form a 1:2 adduct in which the phosphorus center was coordinated to two irons. The failure of ADPO to accept two metal ligands has been previously interpreted in terms of the electron structure of the parent ADPO system [9, 12]. This interpretation is further supported by the iron chemistry reported herein.

One particularly noteworthy feature about the solid state structure of $ADPO{\cdot}Fe(CO)_4$ is the eclipsed arrangement of the axial ADPO group with the equatorial carbonyl groups around the iron. As noted previously (vide supra), the usual arrangement for related phosphine–iron carbonyl complexes would have placed these groups in a staggered configuration. The reason that this eclipsed orientation is adopted by $ADPO{\cdot}Fe(CO)_4$ is unclear. There is no indication of direct interaction of the electron rich ADPO centers with the equatorial carbonyl $\pi$-systems. One possible explanation of this geometry is that the iron tetracarbonyl group has adopted a conformation that could facilitate the edge inversion process [31–37, 12] of the ADPO unit. The adduct of ADPO and $Mn(CO)_2Cp$ ($ADPO{\cdot}Mn(CO)_2Cp$) [9] also shows an orientation in which the best $d$-$\pi$ donor orbital on the manganese is aligned with the ADPO unit in such a way as to stabilize the out-of-plane $p$-orbital that develops at phosphorus during the edge inversion process (Scheme 1). As such the $N{-}P{-}Mn{-}Cp_{(cent.)}$ dihedral angle in $ADPO{\cdot}Mn(CO)_2Cp$ is 79.6° in the solid state.

The iron tetracarbonyl unit in $ADPO{\cdot}Fe(CO)_4$ could be expected to provide a filled $d$-orbital for participation in $p\pi$–$d\pi$ bonding to stabilize the edge inversion transition state at the ligated ADPO. Although the ground state structure of $ADPO{\cdot}Fe(CO)_4$ does not contain a fully developed empty $p$-orbital at phosphorus there may be sufficient electron accepting ability to account for the ground state structural preferences. The structure of $ADPO{\cdot}Mn(CO)_2Cp$ is consistent with such incipient interactions [9].

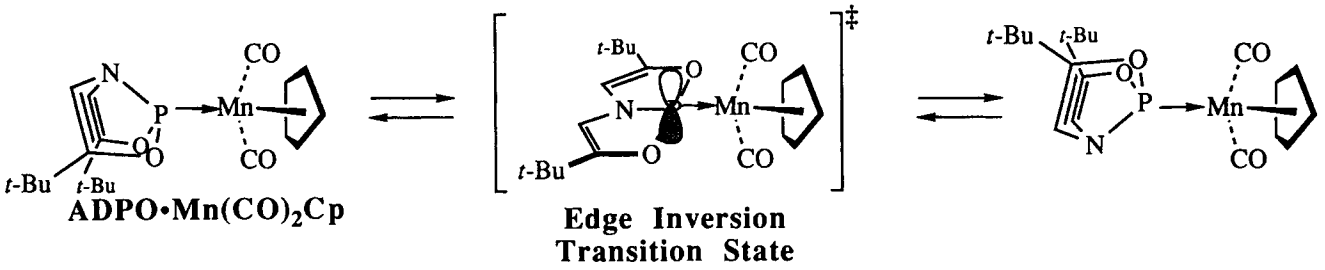


**SCHEME 1**

The iron–phosphorus bond distance and C≡O stretching frequencies in ADPO·Fe(CO)$_4$ also suggest a $\pi$-accepting ability for the folded ADPO ligand (vide supra). Unlike the Mn(CO)$_2$Cp group, the Fe(CO)$_4$ group (as a result of its 3-fold axial symmetry) is not able to provide straightforward geometric evidence that would support an incipient $p\pi$–$d\pi$ interaction. In fact the same iron *d*-orbital is capable of interacting in a $\pi$ sense with a $C_s$ axial substituent (such as folded ADPO) regardless of whether the arrangement is staggered or eclipsed. Since the incipient *p*-orbital at the phosphorus is still heavily involved with the $\sigma$-system about phosphorus at the ground state, the distortion in this orbital may make a distinction between eclipsed and staggered arrangements possible. We decided to investigate this question with the aid of theoretical techniques.

Several calculations on various structures of the 1:1 ADPO:Fe(CO)$_4$ formulation were done in the local density functional (LDF) approximation by using the program system DMol (see Computational Details section). In all calculations the *t*-butyl groups were replaced by a single hydrogen substituent. The calculated geometry parameters of ADPO·Fe(CO)$_4$ (Table 3) are in reasonable agreement with the experimental values. The errors in the structure are similar to those found for the isolated species ADPO (Table 4) and Fe(CO)$_5$ [38] (Table 5). For Fe(CO)$_5$, the calculated Fe–C bond distances are 3 to 6 pm too short. A similar shortening of 3 to 5 pm is found for the Fe–C and Fe–P bonds in ADPO·Fe(CO)$_4$. This shortening of the bonds most likely arises because the LDF method tends to overestimate nonbonding stabilizing interactions and such interactions are known to be important in transition metal complexes. The C–O carbonyl bond lengths are the same as the experimental values within experimental error. In ADPO, the calculated bonds to phosphorus are too long and the remaining bonds are too short. In the complex, the P–N and P–O bonds are calculated to be too long as expected. The C–O and C–N bonds in the ring are too long as compared to experiment (as expected, although the differences are larger than in the isolated molecule). The calculated C–C bonds in the ring are surprisingly longer than the experimental values but are within the experimental error (3 $\sigma$). This result may be due to the omission of the *t*-butyl groups from the calculation. The calculated angles are in good agreement with the experimental values with even the slight twist about the Fe–P bond reproduced by the calculations.

Two structures for ADPO·Fe(CO)$_4$ in which the ADPO unit was planar were also calculated. In the first of these structures, ADPO·Fe(CO)$_4$–TS$_{ax}$, the ADPO unit was in an apical position about the iron (which is the normal position for an unconstrained phosphine-iron carbonyl adduct, vide supra). In ADPO·Fe(CO)$_4$–TS$_{ax}$ the ADPO unit is rotated such

**TABLE 3** Calculated Bond Lengths and Angles in ADPO·Fe(CO)$_4$

| *Bond Length (pm)* | | *Bond Angle (deg.)* | |
|---|---|---|---|
| Fe–P | 211.3 | C–Fe–P | 177.2, 90.8 |
| Fe–C | 176.3, 176.2, 176.8, 176.7 | | 90.7, 87.3 |
| | | Fe–P–N | 125.8 |
| P–O | 166.0, 165.8 | Fe–P–O | 114.1, 114.7 |
| P–N | 174.2 | N–P(fold) | 119.1 |
| C–O$_{ADPO}$ | 138.5, 138.6 | C–C–O | 115.2, 115.3 |
| C≡O | 116.3, 115.9 | C–C–N | 112.9, 112.9 |
| | 116.2, 116.2 | O–P–O | 112.9 |
| | | O–P–N | 93.2, 93.3 |
| C–N | 141.2, 141.2 | C–N–C | 117.4 |
| C–C$_{ring}$ | 133.2, 133.1 | C–Fe–P–N | 7.3, 126.1, −113.1 |

**TABLE 4** Comparison of Experimental and Calculated Bond Lengths and Angles in ADPO

| *Bond Length (pm)* | | | *Bond Angle (deg.)* | | |
|---|---|---|---|---|---|
| | *Expt.*[a] | *Calc.* | | *Expt.*[a] | *Calc.* |
| P–O | 181.4 | 182.6 | O–P–O | 167.7 | 166.8 |
| P–N | 170.3 | 175.6 | O–P–N | 83.8 | 83.4 |
| C–O | 133.0 | 131.8 | C–C–O | 112.6 | 114.3 |
| C–N | 137.8 | 136.9 | C–N–C | 125.2 | 126.1 |
| C–C$_{ring}$ | 134.0 | 135.6 | N–C–C | 111.3 | 110.7 |
| | | | P–N–C | 117.4 | 117.0 |
| | | | P–O–C | 114.8 | 114.7 |

[a] See Reference [4].

**TABLE 5** Comparison of Experimental and Calculated Bond Lengths (pm) in $Fe(CO)_5$

| | *Expt.*[a] | *Calc.* |
|---|---|---|
| $Fe-C_{ax}$ | 177.4 | 180.7 |
| $Fe-C_{eq}$ | 177.2 | 182.7 |
| $C-O_{ax}$ | 115.6 | 115.2 |
| $C-O_{eq}$ | 115.9 | 115.2 |

[a] See Reference [38].

that a unique equatorial C≡O had a 90° dihedral angle with both P–O bonds. Even though a single phosphorus substituent would be expected to occupy an apical site about an iron tetracarbonyl unit, a second planar structure, ADPO·$Fe(CO)_4$–$TS_{eq}$, was considered in order to represent a presumably higher energy point on the energy surface. ADPO–$Fe(CO)_4$–$TS_{eq}$ had the ADPO unit in an equatorial position with the P–O bonds eclipsing the apical C≡O's. The bond lengths and angles in these planar ADPO complexes are presented in Tables 6 and 7. The geometries with planar ring structures are significantly different from that of the ground state. The Fe–P bond is 10 to 12 pm longer than the bond in the bent structure whereas the bonds to the carbonyls show only small changes. The P–N bond is calculated to remain longer in these structures as compared to the calculated value for ADPO. The P–O bonds slightly lengthen from the value in the bent complex toward the value calculated for ADPO. The biggest change is in the backbone, with the C–O bonds in the ring becoming much shorter as compared to the bent complex values and remaining essentially the same as compared to those in ADPO. The C–N and C–C bonds show smaller changes. The angles show significant changes as expected, with the Fe–P–N bond angle becoming linear and the Fe–P–O bond angles decreasing by almost 20°. The O–P–O bond angles significantly increase to a value of 166–167°, which is the same as that in uncomplexed ADPO. The remaining angles are similar to those in free ADPO. The structures of the two planar structures are essentially the same for the ADPO

**TABLE 6** Calculated Bond Lengths and Angles in ADPO·$Fe(CO)_4$–$TS_{ax}$

| *Bond Length (pm)* | | *Bond Angle (deg.)* | |
|---|---|---|---|
| Fe–P | 223.6 | C–Fe–P | 178.6, 91.6, 87.0 |
| Fe–C | 117.1, 176.1, 174.1 | Fe–P–N | 178.6 |
| P–O | 176.0 | Fe–P–O | 96.4 |
| P–N | 174.6 | O–P–N | 83.7 |
| $C-O_{ADPO}$ | 132.8 | C–C–O | 113.2 |
| C≡O | 116.4, 116.2, 116.6 | C–C–N | 109.9 |
| C–N | 136.9 | O–P–O | 167.0 |
| $C-C_{ring}$ | 134.8 | C–N–C | 126.3 |

**TABLE 7** Calculated Bond Lengths and Angles in ADPO·$Fe(CO)_4$–$TS_{eq}$

| *Bond Length (pm)* | | *Bond Angle (deg.)* | |
|---|---|---|---|
| Fe–P | 221.9 | C–Fe–P | 94.0, 118.1 |
| Fe–C | 177.7, 175.6 | Fe–P–N | 180.0 |
| P–O | 178.5 | Fe–P–O | 96.9 |
| P–N | 175.1 | O–P–N | 83.1 |
| $C-O_{ADPO}$ | 132.7 | C–C–O | 113.0 |
| C≡O | 116.4, 115.9 | C–C–N | 110.3 |
| C–N | 137.3 | O–P–O | 166.1 |
| $C-C_{ring}$ | 134.9 | C–N–C | 125.6 |

fragment and differ only in the various angles centered on the Fe atom.

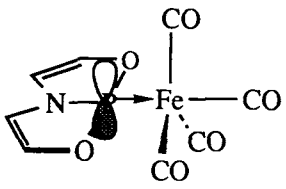


**ADPO•$Fe(CO)_4$-$TS_{ax}$**

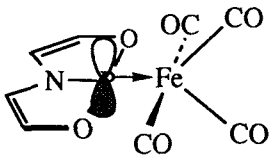


**ADPO•$Fe(CO)_4$-$TS_{eq}$**

The very small energy differences encountered on this potential energy surface are surprising. The lower energy planar structure (ADPO·$Fe(CO)_4$–$TS_{eq}$) is only 0.68 kcal/mol above the energy of the bent structure and the other planar structure (ADPO·$Fe(CO)_4$–$TS_{ax}$) is only 2.40 kcal/mol higher in energy. These small differences are found even though there are significant differences in the geometry parameters. In order to provide further information about the potential energy surface, the carbonyl groups on iron were rotated about the Fe–P bond in the bent structure to yield a "staggered" structure (ADPO·$Fe(CO)_4$–Stag). In this structure the dihedral angle between the N–P bond and an Fe–C bond was 180°. This staggered structure was 0.44 kcal/mol lower in energy than the "eclipsed" structure found in the crystal. One additional structure (ADPO·$Fe(CO)_4$–Mid), which was geometrically midway between the ADPO·$Fe(CO)_4$–$TS_{ax}$ structure and the calculated eclipsed ADPO·$Fe(CO)_4$ ground state structure, was calculated. ADPO·$Fe(CO)_4$–Mid was only 6.1 kcal/mol above the calculated eclipsed ground state structure. Relaxation of the ADPO·$Fe(CO)_4$–Mid structure led toward the folded structure (eclipsed ground state) and the relaxation proceeded very slowly due to the flatness

**TABLE 8** Calculated Energies for Various ADPO·$Fe(CO)_4$ Structures

| *Compound* | *Energy (kcal/mol)* |
|---|---|
| ADPO·$Fe(CO)_4$ | 0.00 |
| ADPO·$Fe(CO)_4$–Stag | −0.44 |
| ADPO·$Fe(CO)_4$–$TS_{eq}$ | 0.68 |
| ADPO·$Fe(CO)_4$–$TS_{ax}$ | 2.40 |
| ADPO·$Fe(CO)_4$–Mid | 6.10 |

of the energy surface. Considering the wide geometric differences between the five calculated structures it is remarkable they are energetically so close (Table 8).

The atomic charges (Table 9) provide some useful insights into the electronic structure. The $Fe(CO)_4$ fragment has charges essentially the same as those in $Fe(CO)_5$. The iron is negative and the carbonyls are slightly positive. The ADPO fragment has some differences in the charge distribution as compared to the uncomplexed molecule. The bent structure has a very positive phosphorus as compared to uncomplexed ADPO. The nitrogen atom is significantly more negative in the bent complex. The oxygen atoms are more negative than found for ADPO and the carbon atoms somewhat more positive. The only difference in the charges of the complexes with planar ADPO and that of the free molecule is the charge on the phosphorus, which is 0.22–0.24 e more positive in the complex.

The flat profile of the ADPO·$Fe(CO)_4$ deformation energy surface is surprising considering the wide variation in geometry that is possible. Our calculations locate a local energy minimum at the geometry (variation in $r_{P-Fe}$ of 12 pm with less than 2.5 kcal/mol change in energy) observed for the X-ray structure of ADPO·$Fe(CO)_4$, but it does not appear to be the global energy minimum since the corresponding staggered structure ADPO·$Fe(CO)_4$–Stag is 0.44 kcal/mol lower in energy. This result could arise from small energy changes due to crystal packing effects or to the additional electronic effects of the *t*-butyl groups present in the

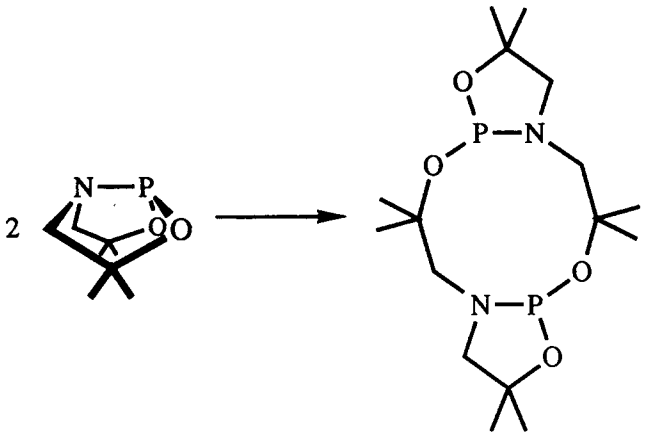


**SCHEME 2**

experimentally studied molecule. In any event, the close energetic positioning of both planar and folded ADPO structures in this iron system suggests that complexes involving planar ADPO units may be observable if the metal center and substitution are chosen carefully.

The adduct $(ADPO)_2Fe(CO)_3$, which contains two ADPO units, is not the simple 2:1 adduct. The two ADPO subunits have dimerized at the iron center. This dimerization of the ADPO fragment is surprising because it is not characteristic of ADPO chemistry. Saturated analogs of ADPO have been observed to dimerize in this fashion [29, 30] without the need for a metal catalyst (Scheme 2), but ADPO has resisted undergoing the analogous reaction.

The dimerization of these [3.3.0]bicyclic systems in this fashion is characteristic of the molecules in which the phosphorus is found in a tetrahedral 8-electron environment (8-P-3 or 8-P-4) rather than the planar 10-electron environment (10-P-3) that is the ground state for ADPO. We have recently observed similar dimerizations in 8-Ge-4 systems [39] that are derived from alkylgermanium trichlorides and the diketoamine ligand [4] from which ADPO is synthesized. The presence of ADPO in an 8-P-4 arrangement in the iron complexes is apparently sufficient to allow dimerization of ADPO units

**TABLE 9** Calculated Charges(e) for Various ADPO·$Fe(CO)_4$ Structures

| *Atom* | *ADPO·$Fe(CO)_4$* | *ADPO·$Fe(CO)_4$–$TS_{eq}$* | *ADPO·$Fe(CO)_4$–$TS_{ax}$* | *ADPO* | *$Fe(CO)_5$* |
|---|---|---|---|---|---|
| Fe | −0.39 | −0.36 | −0.36 | — | −0.36 |
| Fe–*C* | 0.12(eq), 0.16(ax) | 0.12(eq), 0.15(ax) | 0.12(eq), 0.11(eq) 0.15(ax) | — | 0.14(eq), 0.16(ax) |
| C≡*O* | −0.10(eq), −0.09(ax) | −0.10(eq), −0.09(ax) | −0.11(eq), −0.12(eq) −0.10(ax) | — | −0.08(eq), −0.07(ax) |
| P | 0.81 | 0.60 | 0.62 | 0.38 | |
| P–*O* | −0.43 | −0.39 | −0.37 | −0.39 | |
| N | −0.28 | −0.02 | −0.01 | −0.01 | |
| O–*C* | 0.16 | 0.13 | 0.15 | 0.14 | |
| N–*C* | 0.13 | 0.07 | 0.07 | 0.07 | |

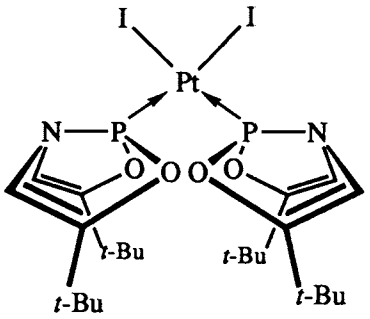


2

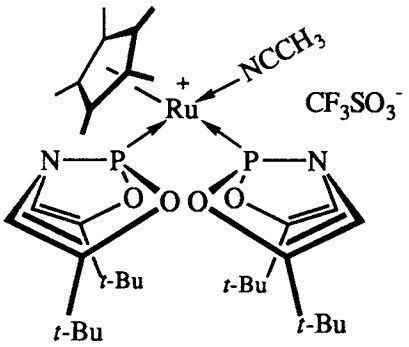


3

when they are in close proximity. The importance of proximity is illustrated by the failure of ADPO units to dimerize in adducts with platinum diiodide [11] (**2**) or pentamethylcyclopentadienylruthenium cation [8] (**3**) in which two units were incorporated at each metal center. The distances between phosphorus centers in the ruthenium and platinum adducts are greater than that in the iron adduct when the ADPO groups occupy an axial and an equatorial position.

In an idealized TBP geometry at an iron center the distance between axial and equatorial phosphorus centers (assuming a P–Fe distance of 215 pm) would be 304 pm. In $(ADPO)_2Fe(CO)_3$ the distance between phosphorus centers is 284 pm in the ADPO dimer unit. The greater bond lengths between phosphorus and platinum result in a P–P distance of 327 pm in *cis*-$(ADPO)_2PtI_2$ (**2**) [11]. Although an X-ray structural study is not available for the *bis*-(ADPO)ruthenium adduct (**3**) [8], a tetrahedral ruthenium coordination complex with two phosphorus centers ((η⁵-pentamethylcyclopentadienyl)(acetonitrile)diphenylsilylene-*bis*(trimethylphosphine)ruthenium tetraphenylborate) [40] shows a P–P distance of 329 pm as a result of increased bond lengths and angles relative to the iron system. The small size of an iron center relative to platinum or ruthenium results in a potentially closer proximity of ADPO units prior to their dimerization. The diaxial disposition of two monomeric ADPO units about a TBP $Fe(CO)_3$ center would be expected to be lower in energy than the axial-equatorial arrangement that is necessary for dimerization. Nonetheless, the rapid pseudorotation at the iron center should make such geometries accessible. In addition to this intramolecular path for dimerization of the ADPO subunits, an intermolecular route can also be envisioned.

When considering an intermolecular route for the dimerization some important factors need to be considered. The ADPO dimer unit has a syn configuration in $(ADPO)_2Fe(CO)_3$ in which both phosphorus lone pairs of electrons (coordinated to iron) are on the same side of the central 10-membered ring. Dimers of the saturated analogs of ADPO have an anti configuration for the phosphorus lone pairs of electrons [29]. The dimers of [3.3.0]bicyclic ring systems containing 8-Ge-4 centers also possess an anti configuration about the central 10-membered ring [39]. Thus, intermolecular dimerizations of [3.3.0]heterobicyclic systems of the type under consideration here appear to give only the anti dimers. The syn dimer of APDO is found in $(ADPO)_2Fe(CO)_3$ as would be expected if the dimerization occurred intramolecularly at a single iron center. The conversion of an intermolecularly formed ADPO anti dimer to the syn isomer could be accomplished if a single phosphorus were free to invert. The inversion of any of these phosphorus centers cannot occur by a traditional vertex inversion mechanism due to the electronegative substituents at phosphorus [31, 33, 35]. The edge inversion process is electronically the most favored pathway in these systems [12, 31–33, 35]. The strict geometric requirements of the edge inversion transition state make it difficult to accommodate in the dimer ring system due to ring strain and steric hindrance. Since conversion of an anti dimer to the syn dimer is energetically unlikely, the direct formation of the syn dimer by an intramolecular dimerization seems the most probable mechanism.

The addition of a third molecule of ADPO to an iron center can be accomplished by photolysis of $(ADPO)_2Fe(CO)_3$ in the presence of additional ADPO. NMR spectra indicate that the third ADPO does not participate in any sort of intramolecular reaction with the ADPO dimer unit. No evidence was observed for the formation of an iron adduct with more than three ADPO units. The most likely explanation for the limit to ADPO incorporation is based on the combined steric requirements of the ADPO dimer unit and the additional (presumably axial) [41–43] ADPO unit. A noteworthy feature of the 3:1 adduct is the chemical shift displacements for the diastereotopic *t*-butyl's ($\Delta\delta$ 0.08) and ring protons ($\Delta\delta$ 0.07) in the independent ADPO group as a result of the influence of the chiral ADPO dimer unit.

## CONCLUSION

Iron carbonyl forms a 1:1 adduct with ADPO that is structurally related to previously studied ADPO transition metal adducts. The ADPO·$Fe(CO)_4$ adduct possesses a highly unusual eclipsed geometry in the solid state. This geometric preference can be understood by consideration of the recently discovered edge inversion process that has been shown to occur at 3- and 4-coordinate main group element centers [32, 36]. Theoretical studies of ADPO·$Fe(CO)_4$ by the LDF technique support the relevance of edge inversion processes in such species.

The addition of a second ADPO molecule to ADPO·$Fe(CO)_4$ results in the formation of an ADPO dimer that is chelated to the iron center. The formation of this dimer by P–O bond rupture and readdition is unprecedented in ADPO chemistry but has been observed previously at 8-electron phosphorus and germanium centers in [3.3.0]bicyclic systems. This dimerization illustrates key electronic differences between 8-P-3 and 10-P-3 bonding arrangements. The importance of proximity effects in this dimerization is illustrated by the failure of **2** and **3** to form such dimer units.

Up to three ADPO units can be incorporated at a single iron carbonyl center. The third ADPO unit does not cyclize with the ADPO dimer unit. The chiral nature of the ADPO dimer unit is revealed by the diastereotopic chemical shifts in the independent ADPO unit of $(ADPO)_2Fe(ADPO)(CO)_2$.

ADPO can be released from ADPO·$Fe(CO)_4$ by the addition of carbon monoxide but the ADPO dimer unit is resistant to such releases.

The flat energy surface calculated for ADPO·$Fe(CO)_4$ deformations suggests that a planar ADPO-metal complex may be possible for some choice of metal and substituents. A structure with more than one isolable minimum energy structure is an intriguing possibility. Work in this area is continuing.

## COMPUTATIONAL METHOD

The calculations were done in the local density functional (LDF) approximation [44–47] by using the program system DMol [48]. The atomic basis functions are given numerically on an atom-centered, spherical-polar mesh. The radial portion of the grid is obtained from the solution of the atomic LDF equations by numerical methods. The radial functions are stored as sets of cubic spline coefficients so that the radial functions are piece-wise analytic, a necessity for the evaluation of gradients. The use of exact spherical atom results offers some advantages. The molecule will dissociate exactly to its atoms within the LDF framework, although this does not guarantee correct dissociation energies. Furthermore, because of the quality of the atomic basis sets, basis set superposition effects should be minimized and correct behavior at the nucleus will be obtained.

Since the basis sets are numerical, the various integrals arising from the expression for the energy need to be evaluated over a grid. The integration points are generated in terms of angular functions and spherical harmonics. The number of radial points $N_R$ is given as: $N_R = 14(Z + 2)^{1/3}$, where $Z$ is the atomic number. The maximum distance for any function is 12 au. The angular integration points $N_0$ are generated at the $N_R$ radial points to form shells around each nucleus. The value of $N_0$ ranges from 14 to 302 depending on the behavior of the density [49]. The Coulomb potential corresponding to the electron repulsion term is determined directly from the electron density by solving Poisson's equation. In DMol, the form for the exchange-correlation energy of the uniform electron gas is that derived by von Barth and Hedin [50].

All of the DMol calculations were done with a double numerical basis set augmented by polarization functions. This can be considered in terms of size as a polarized double zeta basis set. However, because of the use of exact numerical solutions for the atom, this basis set is of significantly higher quality than a normal molecular orbital polarized double zeta basis set. The fitting functions have angular momentum numbers ($l$) one greater than that of the polarization function. All of the atoms except for hydrogen have $d$ polarization functions so that the value of $l$ for the fitting function is 3. For hydrogen with $p$ polarization functions, the value of $l$ for the fitting function is 2.

Geometries were optimized by using analytic gradient methods. There are two problems with evaluating gradients in the LDF framework that are due to the numerical methods that are used. The first is that the energy minimum does not necessarily correspond exactly to the point with a zero derivative. The second is that the sum of the gradients may not always be zero as required for translational invariance. These tend to introduce errors on the order of 0.1 pm in the calculation of the coordinates if both a reasonable grid and basis set are used. This gives bond lengths and angles with reasonable error limits. The difference of 0.1 pm is about an order of magnitude smaller than the accuracy of the LDF geometries as compared to experiment.

## EXPERIMENTAL

Reactions and manipulations were carried out under an atmosphere of dry nitrogen, either in a Vacuum Atmospheres dry box or using standard Schlenk techniques. Solvents were dried (using standard procedures) [51], distilled, and deoxygenated prior to use, unless otherwise indicated. Glassware was oven-dried in a 160°C oven overnight. IR spectra were recorded on a Perkin-Elmer 283 infrared spec-

trophotometer. $^1H$ NMR spectra were recorded on a General Electric QE-300 spectrometer. $^{13}C$ and $^{31}P$ NMR spectra were recorded on a Nicolet NT-300WB spectrometer. NMR references are $(CH_3)_4Si$ ($^1H$, $^{13}C$) and 85% $H_3PO_4$ ($^{31}P$). Mass spectra were obtained on a VGMM 7070 double-focusing high resolution mass spectrometer. Melting points were obtained under nitrogen on a Thomas-Hoover capillary apparatus and are uncorrected. Elemental analyses were performed by Oneida Research Services, Whitesboro, NY, and are within 0.40% of theoretical, unless otherwise indicated.

The iron carbonyl starting materials, $Fe_2(CO)_9$, $Fe(CO)_5$, and $Na_2[Fe(CO)_4]\cdot(\frac{3}{2}$ dioxane), were obtained commercially and used without further purification, except for $Fe(CO)_5$, which was vacuum distilled prior to use. ADPO was synthesized as described previously [4]. Ultraviolet photolyses were carried out in quartz vessels using a Sylvania 275 Watt mercury-arc sunlamp and cooled by a fan.

### *Reaction of ADPO with $Fe_2(CO)_9$*

A flask was charged with $Fe_2(CO)_9$ (1.732 g, 4.761 mmol) and ADPO (1.124 g, 4.659 mmol). Pentane (50 mL) was added and the resulting mixture was stirred for 18 h in the dark. After pumping off the volatiles, the residue was extracted with pentane (10 mL). Pumping off the pentane yielded air-stable (ADPO)$Fe(CO)_4$ as a tan solid: 1.860 g (98%), mp 57–59°C (dec). NMR spectra: $^1H$ ($CD_2Cl_2$) $\delta$ 1.17 (s, 18H), 5.89 (d, $^3J_{PH}$ = 26.4 Hz, 2 H); $^{13}C\{^1H\}$ ($C_6D_{12}$), $\delta$ 27.5 ($CH_3$, s), 32.8 ($C(CH_3)_3$, d, $^3J_{PC}$ = 5.3 Hz), 113.5 (CN, s), 156.4 (COP, d, $J_{PC}$ = 4.9 Hz), 211.4 (FeCO, d, $^2J_{PC}$ = 22.6 Hz); $^{31}P\{^1H\}$ ($C_6D_{12}$), $\delta$ 235. IR spectrum ($cm^{-1}$, pentane): 1977 (vs), 2005 (m), 2070 (m). Mass spectrum (EI): *m/z* 409 ($M^+$, 1.3%), 297 (ADPO·$Fe^+$, base peak). Anal. ($C_{16}H_{20}FeNO_6P$): C, H, N, P.

### *Reaction of ADPO·$Cl_2$ with $Na_2[Fe(CO)_4]$*

A solution of ADPO·$Cl_2$ (0.328 g, 1.05 mmol) in pentane (10 mL) was added dropwise to a stirred slurry of $Na_2[Fe(CO)_4]\cdot(\frac{3}{2}$ dioxane) (0.364 g, 1.05 mmol) in pentane (10 mL) at 0°C. The mixture was allowed to warm to ambient temperature and stirred for 48 h. The $^{31}P$ NMR spectrum showed primarily (ADPO)$Fe(CO)_4$, with several smaller intensity resonances.

### *Photolysis of ADPO with $Fe(CO)_5$*

A solution of ADPO (0.016 g, 0.066 mmol) and $Fe(CO)_5$ (0.013 g, 0.066 mmol) in THF-$d_8$ (1 mL) was irradiated in a quartz NMR tube (sealed with a septum with a needle outlet to a nitrogen bubbler) for 3.5 h. The $^1H$ NMR spectrum indicated the presence of ADPO·$Fe(CO)_4$, with small amounts of $(ADPO)_2Fe(CO)_3$ (vide infra).

### *Photolysis of (ADPO)$Fe(CO)_4$*

A stirred solution of ADPO·$Fe(CO)_4$ (1.012 g, 2.473 mmol) in cyclohexane (35 mL) was irradiated for 60 h. (A precipitate formed during the reaction and the walls of the quartz reaction tube became coated with a residue. This residue was mechanically removed about 40 h into the reaction.) The mixture was then filtered and the volatiles pumped off. Recrystallization of the residue from boiling pentane (10–15 mL) yielded slightly air-sensitive dark brown crystals of $(ADPO)_2Fe(CO)_3$: 0.347 g (45%, based on a theoretical yield of 1.24 mmol), mp 203–206°C. NMR spectra: $^1H$ ($CD_2Cl_2$), $\delta$ 1.15 (s, 18H), 1.22 (s, 18H), 5.58 (pseudo t, spacing = 7.4 Hz, 2H), 5.94 (pseudo t, spacing = 7.0 Hz, 2H); $^{13}C\{^1H\}$ ($C_6D_{12}$), $\delta$ 28.2 ($CH_3$, s), 28.3 ($CH_3$, s), 32.9 ($C(CH_3)_3$, s), 36.1 ($C(CH_3)_3$, s), 110.6 (CN, br), 111.6 (CN, pseudo t, spacing = 6.1 Hz), 143.8 (COP, br), 152.9 (COP, pseudo t, spacing = 6.4 Hz), 214.5 (FeCO, t, $^2J_{PC}$ = 8.8 Hz); $^{31}P\{^1H\}$ ($C_6D_{12}$), $\delta$ 172. IR spectrum ($cm^{-1}$, pentane): 1955 (vs), 1980 (s), 2032 (s). Mass spectrum (EI): *m/z* 622 ($M^+$, 2.0%), 538 [(ADPO)2$Fe^+$, base peak]. Anal. ($C_{16}H_{20}FeNO_6P$): C, H, N, P.

### *Photolysis of ADPO and ADPO·$Fe(CO)_4$*

A solution of ADPO (0.009 g, 0.04 mmol) and (ADPO)$Fe(CO)_4$ (0.015 g, 0.037 mmol) in $C_6D_{12}$ (1 mL) was irradiated in a quartz NMR tube (sealed with a septum with a needle outlet to a nitrogen bubbler) for 2.5 h. The $^{31}P$ NMR spectrum showed the formation of $(ADPO)_2Fe(CO)_3$; however, at this point, significant amounts of $(ADPO)_2Fe(ADPO)(CO)_2$ (vide infra) had formed, and some (ADPO)$Fe(CO)_4$ was still present.

### *Thermal Reaction of ADPO·$Fe(CO)_4$*

A solution of ADPO·$Fe(CO)_4$ (0.100 g, 0.244 mmol) in octane was boiled for 8 h. Integration of the $^{31}P$ NMR spectrum indicated about 10–15% conversion to $(ADPO)_2Fe(CO)_3$. No reaction was observed in boiling cyclohexane.

### *Reaction of (ADPO)$Fe(CO)_4$ with CO*

A solution of (ADPO)$Fe(CO)_4$ (0.057 g, 0.024 mmol) in THF-$d_8$ (1 mL) was heated at 100°C under 135 atmospheres of CO for 12 h. Integration of the $^1H$ NMR spectrum indicated that about 20% of the ADPO was present as the uncomplexed ligand.

### *Attempted Reactions of $(ADPO)_2Fe(CO)_3$ with CO*

A solution of $(ADPO)_2Fe(CO)_3$ (0.060 g, 0.096 mmol) in THF-$d_8$ (1 mL) was heated at 100°C under an atmosphere of 2,000 psi of CO for 12 h. Only $(ADPO)_2Fe(CO)_3$ was observed in the $^{31}P$ NMR spec-

trum. A mixture of $(ADPO)_2Fe(CO)_3$ and $C_6D_{12}$ was shaken at 20°C under 925 atmospheres of CO for 12 h. Only $(ADPO)_2Fe(CO)_3$ was observed in the $^{31}P$ NMR spectrum.

### *Photolysis of ADPO with $(ADPO)_2Fe(CO)_3$*

A solution of ADPO (0.010 g, 0.041 mmol) and $(ADPO)_2Fe(CO)_3$ (0.027 g, 0.043 mmol) in $C_6D_{12}$ (1 mL) was irradiated in a quartz NMR tube (sealed with a septum with a needle outlet to a nitrogen bubbler) for 16 h yielding a light brown solution and dark brown precipitate. $^{31}P$ NMR characterization of the solution indicated the presence of primarily $(ADPO)_2Fe(ADPO)(CO)_2$, with a small amount of $(ADPO)_2Fe(CO)_3$. $(ADPO)_2Fe(ADPO)(CO)_2$ was characterized spectroscopically as a cyclohexane–$D_{12}$ solution. $^1H$ NMR ($C_6D_{12}$): $\delta$ 1.04 (s, $CH_3$, 9H), 1.12 (s, $CH_3$, 9H), 1.14 (s, $CH_3$, 18H), 1.20 (s, $CH_3$, 18H), 5.39 (pseudo t, spacing = 6.9 Hz, [$(ADPO)_2$–NCH], 2H), 5.55 (d, $^3J_{PH}$ = 24.6 Hz, [ADPO–NCH], 1H), 5.62 (d, $^3J_{PH}$ = 24.8 Hz, [ADPO–NCH], 1H), 5.71 (pseudo t, spacing = 6.9 Hz, [$(ADPO)_2$–NCH], 2H). $^{31}P$ NMR ($C_6D_{12}$): $\delta$ 174 (d, $^2J_{PP}$ = 21.7 Hz, [$(ADPO)_2$], 2P), 240 (t, $^2J_{PP}$ = 21.7 Hz, [ADPO], 1P).

### *X-ray Crystal Structure of ADPO·$Fe(CO)_4$*

Formula: $C_{16}H_{20}PNO_6Fe$, monoclinic, space group $P2_1$ (No. 4), $a$ = 1001.8(2), $b$ = 625.0(1), $c$ = 1579.7(3) pm, $\beta$ = 102.69(2)°; $T$ = −70°C, $Z$ = 2, $FW$ = 409.16, $D_c$ = 1.408 g/cm$^3$, $\mu$ (Mo) = 8.89 cm$^{-1}$; Crystal Description: colorless parallelepiped (0.12 × 0.18 × 0.47 mm) grown by pentane evaporation from a solution of ADPO·$Fe(CO)_4$. A total of 1767 reflections were collected, 2.6° ≤ 2$\theta$ ≤ 48.0°, on an Enraf-Nonius CAD4 diffractometer with graphite monochromator using Mo-$K_\alpha$ radiation ($\lambda$ = 71.073 pm). With 1031 unique reflections of intensity greater than 3.0 $\sigma$, the structure was solved by automated Patterson analysis (PHASE) and standard difference Fourier techniques. There were 225 parameters with all nonhydrogen atoms anisotropic and all hydrogens in fixed positions. The final $R$ factors were 0.040, $R_w$ = 0.040. The final difference Fourier showed the largest residual density to be 0.45 e/Å$^3$ (background).

### *X-ray Crystal Structure of $(ADPO)_2Fe(CO)_3$*

Formula: $C_{27}H_{40}P_2N_2O_7Fe·C_4H_{10}O$, triclinic, space group $P_1$(No. 2) $a$ = 1089.2(3), $b$ = 1729.0(3), $c$ = 1080.0(2) pm, $\alpha$ = 95.04(1)°, $\beta$ = 111.80(1)°, $\gamma$ = 78.82(1)°; $T$ = −100°C, $Z$ = 2, $FW$ = 696.54, $D_c$ = 1.249 g/cm$^3$, $\mu$ (Mo) = 5.35 cm$^{-1}$; Crystal Description: pale yellow, parallelepiped (0.32 × 0.31 × 0.40 mm) grown from cyclohexane/diethyl ether by cooling. A total of 5636 reflections were collected, 11.3° ≤ 2$\theta$ ≤ 50.0°, on a Syntex R3 diffractometer with graphite monochromator using Mo-$K_\alpha$ radiation ($\lambda$ = 71.073 pm). With 3887 unique reflections of intensity greater than 3.0 $\sigma$, the structure was solved by automated Patterson analysis (PHASE) and standard difference Fourier techniques. The independent unit consists of one $(ADPO)_2Fe(CO)_3$ molecule and a disordered diethyl ether molecule in general positions. The ether disorder was treated by splitting one methylene group between two half-atoms. The second methylene was more satisfactorily modeled via thermal parameters. There were 406 parameters with all nonhydrogen atoms anisotropic and hydrogens in fixed positions. The final $R$ factors were $R$ = 0.034, $R_w$ = 0.037. The final difference Fourier showed the largest residual density to be 0.56 e/Å$^3$, near the disordered diethyl ether solvate. Atomic coordinates, bond lengths, angles and thermal parameters are available in supplementary material.

## *ACKNOWLEDGMENT*

Acknowledgment is made to J. E. Feaster for his excellent technical assistance. We also appreciate the helpful discussions with Drs. H. V. R. Dias and C. A. Stewart concerning the mechanism of formation of the ADPO dimer.

## *SUPPLEMENTARY MATERIAL AVAILABLE*

A complete description of the X-ray crystallographic structure determinations on ADPO·$Fe(CO)_4$ and $(ADPO)_2Fe(CO)_3$ has been deposited with the Cambridge Crystallographic Data Centre.

## *REFERENCES AND NOTES*

[1] S. A. Culley, A. J. Arduengo, III, *J. Am. Chem. Soc., 106,* 1984, 1164.
[2] S. A. Culley, A. J. Arduengo, III, *J. Am. Chem. Soc., 107,* 1985, 1089.
[3] C. A. Stewart, R. L. Harlow, A. J. Arduengo, III, *J. Am. Chem. Soc., 107,* 1985, 5543.
[4] A. J. Arduengo, III, C. A. Stewart, F. Davidson, D. A. Dixon, J. Y. Becker, S. A. Culley, M. B. Mizen, *J. Am. Chem. Soc., 109,* 1987, 627.
[5] A. J. Arduengo, III, U.S. Patent 4710576 (1987).
[6] A. J. Arduengo, III, *Pure & Appl. Chem., 59,* 1987, 1053.
[7] A. J. Arduengo, III, D. A. Dixon, C. A. Stewart, *Phos. and Sulfur, 30,* 1987, 341.
[8] A. J. Arduengo, III, M. Lattman, J. C. Calabrese, P. J. Fagan, *Heteroatom Chem., 1,* 1990, 407.
[9] A. J. Arduengo, III, M. Lattman, H. V. R. Dias, J. C. Calabrese, M. Kline, *J. Am. Chem. Soc., 113,* 1991, 1799.
[10] C. A. Stewart, A. J. Arduengo, III, *Inorg. Chem., 25,* 1986, 3847.
[11] A. J. Arduengo, III, C. A. Stewart, F. Davidson, *J. Am. Chem. Soc., 108,* 1986, 322.

[12] A. J. Arduengo, D. A. Dixon: Electron Rich Bonding at Low Coordination Main Group Element Centers, in E. Block (Ed.): *Heteroatom Chemistry: ICHAC-2*, VCH, New York, p. 47 (1990).
[13] D. A. Dixon, A. J. Arduengo, III, *Phos. and Sulf., 55*, 1991, 35.
[14] The *N-X-L* nomenclature system has been previously described (C. W. Perkins, J. C. Martin, A. J. Arduengo, III, W. Lau, A. Algeria, J. K. Kochi, *J. Am. Chem. Soc., 102*, 1980, 7753). *N* valence electrons about a central atom *X*, with *L* ligands.
[15] The ADPnO acronym has been previously described and is used for simplicity in place of the name of the ring system it represents: 5-*aza*-2,8-*dioxa*-1-*pnicta*-bicyclo[3.3.0]*octa*-2,4,6-triene. See reference 4, footnote 1d for details.
[16] D. F. Shriver, K. H. Whitmire: Iron Compounds without Hydrocarbon Ligands, in G. Wilkinson, F. G. A. Stone, E. W. Abel, (Eds.): *Comprehensive Organometallic Chemistry*, Pergamon, Oxford, p. 289 (1982).
[17] A. Reckziegel, M. Bigorgne, *J. Organomet. Chem., 3*, 1965, 341.
[18] R. B. King, *Inorg. Chem., 2*, 1963, 936.
[19] L. J. Todd, J. R. Wilkinson, *J. Organomet. Chemistry, 77*, 1974, 1.
[20] M. Akhtar, P. D. Ellis, A. G. MacDiarmid, J. D. Odom, *Inorg. Chem., 11*, 1972, 2917.
[21] This drawing was made with the *KANVAS* computer graphics program. This program is based on the program *SCHAKAL* of E. Keller (Kristallographisches Institute der Universitat Freiburg, FRG), which was modified by A. J. Arduengo, III (E. I. du Pont de Nemours & Co., Wilmington, DE) to produce the back and shadowed planes. The planes bear a 50-pm grid and the lighting source is at infinity so that shadow size is meaningful.
[22] A. H. Cowley, R. E. Davis, K. Remadna, *Inorg. Chem., 20*, 1981, 2146.
[23] P. E. Riley, R. E. Davis, *Inorg. Chem., 19*, 1980, 159.
[24] B. T. Kilbourn, U. A. Raeburn, D. T. Thompson, *J. Chem. Soc. (A)*, 1969, 1906.
[25] D. W. Bennett, R. J. Neustadt, R. W. Parry, F. W. Cagle, Jr., *Acta Cryst., B34*, 1978, 3362.
[26] P. Vierling, J. G. Riess, A. Grand, *Inorg. Chem., 25*, 1986, 4144.
[27] A. H. Cowley, R. E. Davis, M. Lattman, M. McKee, K. Remadna, *J. Am. Chem. Soc., 101*, 1979, 5090.
[28] The CH $^{1}H$, CN and COP $^{13}C$ resonances appear as triplets due to coupling to chemically equivalent, but magnetically inequivalent, phosphorus atoms that give rise to an AA'X (or ABX) spin system. For a discussion of these observations in a related complex, $[(CH_3)_2PCH_2CH_2P(CH_3)_2]Fe(CO)_3$, see ref. 20.
[29] C. Bonningue, D. Houalla, R. Wolf, *J. Chem. Soc., Perkin Trans., II*, 1983, 773.
[30] C. Bonningue, D. Houalla, M. Sanchez, R. Wolf, *J. Chem. Soc., Perkin Trans. II*, 1981, 19.
[31] D. A. Dixon, A. J. Arduengo, III, T. Fukunaga, *J. Am. Chem. Soc., 108*, 1986, 2461.
[32] A. J. Arduengo, III, D. A. Dixon, D. C. Roe, *J. Am. Chem. Soc., 108*, 1986, 6821.
[33] D. A. Dixon, A. J. Arduengo, III, *J. Am. Chem. Soc., 109*, 1987, 338.
[34] D. A. Dixon, A. J. Arduengo, III, *J. Phys. Chem., 91*, 1987, 3195.
[35] D. A. Dixon, A. J. Arduengo, III, *J. Chem. Soc., Chem. Commun., 1987*, 1987, 498.
[36] A. J. Arduengo, III, D. A. Dixon, D. C. Roe, M. Kline, *J. Am. Chem. Soc., 110*, 1988, 4437.
[37] D. A. Dixon, A. J. Arduengo, III, *Int. J. Quant. Chem. (Quant. Chem. Symp. 22)*, 1988, 85.
[38] B. Beagley, D. G. Schmidling, *J. Mol. Struct., 22*, 1974, 466.
[39] A. J. Arduengo, III, G. Bettermann, J. Breker, unpublished results.
[40] D. A. Straus, T. D. Tilley, A. L. Rheingold, S. J. Geib, *J. Am. Chem. Soc., 109*, 1987, 5872.
[41] H. Berke, W. Bankhardt, G. Huttner, J. von Seyerl, L. Zsolnai, *Chem. Ber., 114*, 1981, 2754.
[42] L. P. Battaglia, G. P. Chiusoli, M. Nardelli, C. Pelizzi, G. Predieri, *Gazz. Chim. Ital., 116*, 1986, 207.
[43] A. B. Burg, *Inorg. Chem., 25*, 1986, 4751.
[44] R. G. Parr, W. Yang: *Density Functional Theory of Atoms and Molecules;* Oxford University Press, New York, 1989.
[45] D. R. Salahub in: *Ab Initio Methods in Quantum Chemistry-II, Ed.*, Wiley, New York, p. 447 (1987).
[46] E. Wimmer, A. J. Freeman, C.-L. Fu, P.-L. Cao, S.-H. Chou, B. Delley in K. F. Jensen, D. G. Truhlar (eds.): *Supercomputer Research in Chemistry and Chemical Engineering*, ACS Symposium Series No. 353, American Chemical Society, Washington, D.C., p. 49 (1987).
[47] R. O. Jones, O. Gunnarsson, *Rev. Mod. Phys., 61*, 1989, 689.
[48] B. J. Delley, *J. Chem. Phys., 92*, 1990, 508. DMol is available commercially from Biosym Technologies, San Diego, CA.
[49] This grid can be obtained by using the FINE command in DMOL.
[50] U. von Barth, L. Hedin, *J. Phys. C, 5*, 1972, 1629.
[51] D. D. Perrin, W. L. F. Armarego, D. R. Perrin: *Purification of Laboratory Chemicals*, Pergamon, New York, 1985.